Transonic Correction to Theodorsen's Theory for Oscillating Airfoil in Pitch and Plunge Toward Flutter

Nhan Nguyen*
NASA Ames Research Center, Moffett Field, CA 94035
Juntao Xiong†
KBR Wyle, Inc., Moffett Field, CA 94035

This paper presents a transonic correction method for an oscillating airfoil in pitch and plunge. The proposed method applies correction functions to the Theodorsen's theory to capture the transonic nonlinear aerodynamics. These correction functions apply necessary corrections to the amplitudes and the phase angles of the unsteady lift and pitching moment coefficients to account for transonic aerodynamics. The proposed method also postulates a correction for the motion of the aerodynamic center which could be induced by moving shocks. A series of unsteady RANS CFD simulations of the airfoil at the mean aerodynamic chord of the Transonic Truss-Braced Wing aircraft are conducted using FUN3D to provide data to construct these transonic correction functions. The computed responses of the unsteady lift and pitching moment coefficients using these transonic correction functions match the CFD simulation results very well even when the pitching moment coefficient is highly nonlinear. A flutter analysis of an airfoil in pitch and plunge illustrates the potential use of the proposed transonic correction method.

I. Introduction

Transonic flutter is a current topic of high interest in aircraft design. Flutter clearance certification for transport aircraft requires flight testing and flutter analysis. The doublet lattice method[1] is the industry standard tool for flutter analysis of aerospace vehicles. It is widely used in flutter prediction for subsonic flow. In transonic flow, correction methods to the doublet lattice method are typically employed by means of correcting the lift curve slope of a doublet lattice model with the lift curve slope obtained from a high-fidelity computational fluid dynamics (CFD) simulation. Three-dimensional (3D) unsteady Reynolds averaged Navier-Stokes (RANS) methods for transonic flutter have also been developed.[2] The 3D unsteady RANS methods provide increased accuracy in flutter prediction but usually at the steep expense of computational efficiency. In many applications that involve design optimization with flutter constraints, the computational cost associated with high-fidelity CFD method presents a barrier. Therefore, computationally efficient methods for transonic flutter prediction continue to be of high interest to the aircraft design community. In recent years, there have been new approaches to developing reduced-order models for transonic flutter.[3]

In the present study, a new method for extending the classical Theodorsen's theory[4] of unsteady aerodynamics for incompressible flow to transonic flow is proposed. The method proposes a modified Theodorsen's function to correct for changes in the amplitude and phase shift of the lift and pitching moment of an oscillating airfoil in transonic flow. The amplitude and phase shift corrections are generally a function of the flow parameters such as the Mach number, the reduced frequency, and the instantaneous angle of attack as well the airfoil characteristics such as the thickness and the type of airfoil. To derive the unsteady corrections, unsteady CFD simulations are performed using FUN3D for selected reduced frequencies and Mach numbers for a number of transonic airfoils of the Boeing Transonic Truss-Braced Wing aircraft configuration.[5,6]

In previous studies, this transonic correction method is first introduced by the author but it only corrects for the unsteady circulatory lift while the non-circulatory lift is assumed to be unaffected by transonic flow.[7–9] This

*Senior Research Scientist and Technical Group Lead of Advanced Control and Engineering Systems Group, Intelligent Systems Division, nhan.t.nguyen@nasa.gov
†Aerospace Engineer, Intelligent System Division, juntao.xiong@nasa.gov

assumption is considered to be unsatisfactory. The previous studies also do not address the transonic correction for the unsteady transonic pitching moment. In the current investigation, the transonic effect on the non-circulatory lift is included. A nonlinear model of the pitching moment is developed for the transonic correction. The nonlinearity of the pitching moment observed in the CFD results is modeled as the unsteady motion of the aerodynamic center. This model demonstrates an excellent agreement with the CFD results. A two-dimensional flutter analysis of an airfoil in transonic flow is investigated to illustrate the nonlinear transonic effect on flutter.

II. Transonic Correction Method for Oscillating Airfoil in Pitch

Consider an oscillating airfoil with a sinusoidal angle of attack

$$\alpha = \bar{\alpha} + \tilde{\alpha} \tag{1}$$

$$\tilde{\alpha} = \alpha_0 \sin \omega t = \alpha_0 \sin k\tau \tag{2}$$

where $\tau = \frac{2V_\infty t}{c}$ is a non-dimensional time and $k = \frac{\omega c}{2V_\infty}$ is the reduced frequency.

A. Unsteady Lift Transonic Correction

The unsteady lift coefficient is expressed as

$$c_l = \bar{c}_l + \tilde{c}_l \tag{3}$$

where $\bar{c}_l = c_{l_0} + c_{l_\alpha}\bar{\alpha}$ is the steady-state lift coefficient and $\tilde{c}_l$ is the unsteady lift coefficient.

We propose an unsteady transonic correction to the unsteady lift coefficient of the form

$$\tilde{c}_l = (U_\alpha + iW_\alpha)\frac{c_{l_\alpha}}{c_{l_\alpha^*}}\tilde{c}_l^* \tag{4}$$

where $U_\alpha(k, M_\infty, \bar{\alpha}, \alpha_0)$ and $W_\alpha(k, M_\infty, \bar{\alpha}, \alpha_0)$ are transonic correction functions to be applied to the Theodorsen's unsteady lift coefficient, denoted by $\tilde{c}_l^*$, of an oscillating airfoil in incompressible flow, $c_{l_\alpha}^* = 2\pi$, and c_{l_α} is the steady-state lift curve slope. The complex-valued correction provides both the amplitude and phase corrections to the unsteady lift by the functions $U_\alpha(k, M_\infty, \bar{\alpha}, \alpha_0)$ and $W_\alpha(k, M_\infty, \bar{\alpha}, \alpha_0)$, respectively. These functions depend on the reduced frequency k, Mach number M_∞, the mean angle of attack $\bar{\alpha}$, the amplitude of the alternating component of the angle of attack α_0, and the airfoil geometry.

The unsteady lift coefficient $\tilde{c}_l^*$ is established by the Theodorsen's theory as

$$\tilde{c}_l^* = c_{l_c}^* + c_{l_{nc}}^* \tag{5}$$

where $c_{l_c}^*$ is the circulatory lift coefficient and $c_{l_{nc}}^*$ is the non-circulatory lift coefficient for incompressible flow.

The circulatory lift coefficient $c_{l_c}^*$ for incompressible flow is given by

$$c_{l_c}^* = C(k)\, c_{l_\alpha}^* \left(\tilde{\alpha} + 2\frac{e_c}{c}\frac{c\dot{\alpha}}{2V_\infty}\right) = [F(k) + iG(k)]\, c_{l_\alpha}^* \left(\tilde{\alpha} + 2\frac{e_c}{c}\frac{d\alpha}{d\tau}\right) \tag{6}$$

where $C(k)$ is the complex-valued Theodorsen's function.

For a harmonic motion with $\theta = e^{ik\tau}$, we have $\frac{d\theta}{d\tau} = ik\theta$ and $\frac{d^2\theta}{d\tau^2} = ik\frac{d\theta}{d\tau} = -k^2\theta$. Then,

$$\begin{aligned}
c_{l_c}^* &= F(k)\, c_{l_\alpha}^* \left(\tilde{\alpha} + 2\frac{e_c}{c}\frac{d\alpha}{d\tau}\right) + \frac{1}{k}G(k)\, c_{l_\alpha}^* \left(ik\tilde{\alpha} + 2\frac{e_c}{c}ik\frac{d\alpha}{d\tau}\right) \\
&= F(k)\, c_{l_\alpha}^* \left(\tilde{\alpha} + 2\frac{e_c}{c}\frac{d\alpha}{d\tau}\right) + \frac{1}{k}C_G G(k)\, c_{l_\alpha}^* \left(\frac{d\alpha}{d\tau} - 2k^2\frac{e_c}{c}\tilde{\alpha}\right) \\
&= \left[F(k) - 2k\frac{e_c}{c}G(k)\right] c_{l_\alpha}^* \tilde{\alpha} + \left[G(k) + 2k\frac{e_c}{c}F(k)\right]\frac{1}{k}c_{l_\alpha}^*\frac{d\alpha}{d\tau} \\
&= c_{l_\alpha}^* \alpha_0 \left[F(k) - 2k\frac{e_c}{c}G(k)\right]\sin k\tau + c_{l_\alpha}^* \alpha_0 \left[G(k) + 2k\frac{e_c}{c}F(k)\right]\cos k\tau
\end{aligned} \tag{7}$$

The non-circulatory lift coefficient $c^*_{l_{nc}}$ for incompressible flow is due to the inertial force acting on the oscillating airfoil and is given by

$$c^*_{l_{nc}} = \pi \frac{c\dot{\alpha}}{2V_\infty} + 2\pi \frac{e_m}{c} \frac{c^2 \ddot{\alpha}}{4V_\infty^2} = \pi \frac{d\alpha}{d\tau} + 2\pi \frac{e_m}{c} \frac{d^2\alpha}{d\tau^2} = \pi k \alpha_0 \left(\cos k\tau - 2k \frac{e_m}{c} \sin k\tau \right) \tag{8}$$

The unsteady lift coefficient $\tilde{c}^*_l$ for incompressible flow is obtained by adding the circulatory lift coefficient and the non-circulatory lift coefficient together, resulting in

$$\tilde{c}^*_l = c^*_{l_\alpha} \alpha_0 \left(F_k \sin k\tau + G_k \cos k\tau \right) \tag{9}$$

where

$$F_k = F(k) - 2k \frac{e_c}{c} G(k) - k^2 \frac{e_m}{c} \tag{10}$$

$$G_k = G(k) + 2k \frac{e_c}{c} F(k) + \frac{k}{2} \tag{11}$$

The unsteady lift coefficient with the transonic correction is then expressed as

$$\tilde{c}_l = c_{l_\alpha} \alpha_0 \left(F_k U_\alpha - G_k W_\alpha \right) \sin k\tau + c_{l_\alpha} \alpha_0 \left(F_k W_\alpha + G_k U_\alpha \right) \cos k\tau \tag{12}$$

The Fourier sine and cosine transforms of the unsteady lift coefficient are computed as

$$\int_0^{\frac{2n\pi}{k}} \tilde{c}_l \sin k\tau d\tau = \frac{n\pi}{k} c_{l_\alpha} \alpha_0 \left(F_k U_\alpha - G_k W_\alpha \right) \tag{13}$$

$$\int_0^{\frac{2n\pi}{k}} \tilde{c}_l \cos k\tau d\tau = \frac{n\pi}{k} c_{l_\alpha} \alpha_0 \left(G_k U_\alpha + F_k W_\alpha \right) \tag{14}$$

where n is the number of periods of oscillation.

Thus, the transonic amplitude and phase lift correction functions U_α and W_α can be obtained from the Fourier sine and cosine transforms of the unsteady lift coefficient as

$$U_\alpha = \frac{k \left(F_k \int_0^{\frac{2n\pi}{k}} \tilde{c}_l \sin k\tau d\tau + G_k \int_0^{\frac{2n\pi}{k}} \tilde{c}_l \cos k\tau d\tau \right)}{n\pi c_{l_\alpha} \alpha_0 \left(F_k^2 + G_k^2 \right)} \tag{15}$$

$$W_\alpha = \frac{k \left(F_k \int_0^{\frac{2n\pi}{k}} \tilde{c}_l \cos k\tau d\tau - G_k \int_0^{\frac{2n\pi}{k}} \tilde{c}_l \sin k\tau d\tau \right)}{n\pi c_{l_\alpha} \alpha_0 \left(F_k^2 + G_k^2 \right)} \tag{16}$$

B. Unsteady Pitching Moment Transonic Correction

The Theodorsen's theory establishes the pitching moment coefficient about the pitch center as

$$c_m = \bar{c}_m + c_{m_c} + c_{m_{nc}} \tag{17}$$

where $\bar{c}_m$ is the steady-state pitching moment coefficient, c_{m_c} is the circulatory pitching moment coefficient, and $c_{m_{nc}}$ is the non-circulatory pitching moment coefficient.

For incompressible flow, the aerodynamic center is at the quarter-chord point. For supersonic flow, the aerodynamic center moves to the mid-chord point. Thus, for transonic flow, the aerodynamic center moves between the quarter-chord and mid-chord points. The motion of the aerodynamic center may be modeled as

$$x_{ac} = \bar{x}_{ac} + x_0 \sin(\omega t - \phi) = \bar{x}_{ac} + x_0 \sin(k\tau - \phi) \tag{18}$$

where ϕ is the phase delay angle between the angle of attack motion and the aerodynamic center motion. We make an assumption that the unsteady motion of the aerodynamic center is proportional to the unsteady angle of attack such that

$$\frac{x_{ac}}{c} = \frac{\bar{x}_{ac}}{c} + (A_\alpha + iB_\alpha) \frac{\tilde{\alpha}}{\alpha_0} \tag{19}$$

where the functions $A_\alpha(k, M_\infty, \bar{\alpha}, \alpha_0)$ and $B_\alpha(k, M_\infty, \bar{\alpha}, \alpha_0)$ represent the amplitude and phase angle of the motion of the aerodynamic center.

The steady-state pitching moment coefficient about the pitch center can be expressed as

$$\bar{c}_m = c_{m_{ac}} + \frac{\bar{e}}{c}\bar{c}_l \tag{20}$$

where $\bar{e} = x_e - \bar{x}_{ac}$ is the distance between the pitch center and mean aerodynamic center.

From the steady-state aerodynamics, we obtain

$$\frac{\partial \bar{c}_m}{\partial \bar{\alpha}} = \frac{\partial c_{m_{ac}}}{\partial \bar{\alpha}} + \frac{\bar{e}}{c}c_{l_\alpha} \tag{21}$$

By the definition of an aerodynamic center, $\frac{\partial c_{m_{ac}}}{\partial \bar{\alpha}} = 0$. Therefore, we write

$$\bar{c}_m = \bar{c}_{m_0} + c_{m_\alpha}\bar{\alpha} \tag{22}$$

where $\bar{c}_{m_0} = c_{m_{ac}} + \frac{\bar{e}}{c}\bar{c}_{l_0}$ is the pitching moment coefficient about the pitch center at the zero angle of attack and c_{m_α} is the pitching moment curve slope about the pitch center.

Using the pitching moment curve slope c_{m_α}, the distance $\bar{e}$ between the pitch center and mean aerodynamic center can be determined as

$$\frac{\bar{e}}{c} = \frac{c_{m_\alpha}}{c_{l_\alpha}} \tag{23}$$

Then, the pitching moment coefficient about the aerodynamic center is obtained as

$$c_{m_{ac}} = \bar{c}_m - \frac{c_{m_\alpha}}{c_{l_\alpha}}\bar{c}_l \tag{24}$$

The circulatory pitching moment coefficient about the pitch center is given by

$$c_{m_c} = (x_e - x_{ac})\, c_{l_c} = \left[\frac{\bar{e}}{c} - (A_\alpha + iB_\alpha)\frac{\tilde{\alpha}}{\alpha_0}\right] c_{l_c} \tag{25}$$

The circulatory lift coefficient is computed as

$$c_{l_c} = (U_\alpha + iW_\alpha)\frac{c_{l_\alpha}}{c_{l^*_\alpha}} c^*_{l_c} = F_c \sin k\tau + G_c \cos k\tau \tag{26}$$

where

$$F_c = c_{l_\alpha}\alpha_0 \left[F(k) - 2k\frac{e_c}{c}G(k)\right] U_\alpha - c_{l_\alpha}\alpha_0 \left[G(k) + 2k\frac{e_c}{c}F(k)\right] W_\alpha \tag{27}$$

$$G_c = c_{l_\alpha}\alpha_0 \left[G(k) + 2k\frac{e_c}{c}F(k)\right] U_\alpha + c_{l_\alpha}\alpha_0 \left[F(k) - 2k\frac{e_c}{c}G(k)\right] W_\alpha \tag{28}$$

Then, the circulatory pitching moment coefficient about the pitch center is obtained as

$$\begin{aligned}
c_{m_c} =& \left[\frac{\bar{e}}{c} - (A_\alpha + iB_\alpha)\frac{\tilde{\alpha}}{\alpha_0}\right](F_c \sin k\tau + G_c \cos k\tau) \\
=& \frac{\bar{e}}{c}(F_c \sin k\tau + G_c \cos k\tau) \\
& - \sin k\tau \left[F_c (A_\alpha \sin k\tau + B_\alpha \cos k\tau) + G_c (A_\alpha \cos k\tau - B_\alpha \sin k\tau)\right] \\
=& \frac{\bar{e}}{c}F_c \sin k\tau + \frac{\bar{e}}{c}G_c \cos k\tau - (F_c A_\alpha - G_c B_\alpha)\sin^2 k\tau - \frac{1}{2}(G_c A_\alpha + F_c B_\alpha)\sin 2k\tau \\
=& \frac{\bar{e}}{c}F_c \sin k\tau + \frac{\bar{e}}{c}G_c \cos k\tau - \frac{1}{2}(F_c A_\alpha - G_c B_\alpha) \\
& + \frac{1}{2}(F_c A_\alpha - G_c B_\alpha)\cos 2k\tau - \frac{1}{2}(G_c A_\alpha + F_c B_\alpha)\sin 2k\tau
\end{aligned} \tag{29}$$

It is interesting to note that the circulatory pitching moment coefficient produces a steady-state component equal to $-\frac{1}{2}(F_c A_\alpha - G_c B_\alpha)$ due to the unsteady lift coefficient and the motion of the aerodynamic center. The second harmonic

of the frequency response of the circulatory pitching moment coefficient is a nonlinear term due to the product of the unsteady angle of attack and unsteady lift.

We also propose a transonic correction for the non-circulatory pitching moment coefficient as

$$c_{m_{nc}} = (T_\alpha + iV_\alpha)\, c^*_{m_{nc}} \tag{30}$$

where $c^*_{m_{nc}}$ is the non-circulatory pitching moment coefficient for incompressible flow given by the Theodorsen's theory as

$$\begin{aligned} c^*_{m_{nc}} &= -\pi \frac{e_c}{c} \frac{c\dot{\alpha}}{2V_\infty} - \frac{\pi}{16}\left(1+32\frac{e_m^2}{c^2}\right)\frac{c^2\ddot{\alpha}}{4V_\infty^2} = -\pi\frac{e_c}{c}\frac{d\alpha}{d\tau} - \frac{\pi}{16}\left(1+32\frac{e_m^2}{c^2}\right)\frac{d^2\alpha}{d\tau^2} \\ &= \pi k\alpha_0\left[\frac{k}{16}\left(1+32\frac{e_m^2}{c^2}\right)\sin k\tau - \frac{e_c}{c}\cos k\tau\right] \end{aligned} \tag{31}$$

Thus,

$$c_{m_{nc}} = \pi k\alpha_0\left[\frac{k}{16}\left(1+32\frac{e_m^2}{c^2}\right)(T_\alpha \sin k\tau + V_\alpha \cos k\tau) - \frac{e_c}{c}(T_\alpha \cos k\tau - V_\alpha \sin k\tau)\right] \tag{32}$$

Summing all the contributions of the pitching moment coefficient, the unsteady pitching moment coefficient is obtained as

$$\tilde{c}_m = F_m \sin k\tau + G_m \cos k\tau - \frac{1}{2}(G_c A_\alpha + F_c B_\alpha)\sin 2k\tau + \frac{1}{2}(F_c A_\alpha - G_c B_\alpha)\cos 2k\tau \tag{33}$$

where

$$F_m = \frac{\bar{e}}{c}F_c + \pi k\alpha_0\left[\frac{k}{16}\left(1+32\frac{e_m^2}{c^2}\right)T_\alpha + \frac{e_c}{c}V_\alpha\right] \tag{34}$$

$$G_m = \frac{\bar{e}}{c}G_c + \pi k\alpha_0\left[\frac{k}{16}\left(1+32\frac{e_m^2}{c^2}\right)V_\alpha - \frac{e_c}{c}T_\alpha\right] \tag{35}$$

The Fourier sine and cosine transforms of the unsteady pitching moment coefficients are computed as

$$\int_0^{\frac{2n\pi}{k}} \tilde{c}_m \sin k\tau d\tau = \frac{n\pi}{k}F_m \tag{36}$$

$$\int_0^{\frac{2n\pi}{k}} \tilde{c}_m \cos k\tau d\tau = \frac{n\pi}{k}G_m \tag{37}$$

$$\int_0^{\frac{2n\pi}{k}} \tilde{c}_m \sin 2k\tau d\tau = -\frac{n\pi}{2k}(G_c A_\alpha + F_c B_\alpha) \tag{38}$$

$$\int_0^{\frac{2n\pi}{k}} \tilde{c}_m \cos 2k\tau d\tau = \frac{n\pi}{2k}(F_c A_\alpha - G_c B_\alpha) \tag{39}$$

Thus, the transonic correction functions A_α, B_α, T_α, and V_α can be obtained from the Fourier sine and cosine transforms of the unsteady pitching moment coefficient as

$$A_\alpha = \frac{2k\left(F_c\int_0^{\frac{2n\pi}{k}}\tilde{c}_m\cos 2k\tau d\tau - G_c\int_0^{\frac{2n\pi}{k}}\tilde{c}_m\sin 2k\tau d\tau\right)}{n\pi(F_c^2+G_c^2)} \tag{40}$$

$$B_\alpha = -\frac{2k\left(F_c\int_0^{\frac{2n\pi}{k}}\tilde{c}_m\sin 2k\tau d\tau + G_c\int_0^{\frac{2n\pi}{k}}\tilde{c}_m\cos 2k\tau d\tau\right)}{n\pi(F_c^2+G_c^2)} \tag{41}$$

$$T_\alpha = \frac{\frac{k}{16}\left(1+32\frac{e_m^2}{c^2}\right)\left(F_m - \frac{\bar{e}}{c}F_c\right) - \frac{e_c}{c}\left(G_m - \frac{\bar{e}}{c}G_c\right)}{\pi k\alpha_0\left[\left(\frac{k}{16}\right)^2\left(1+32\frac{e_m^2}{c^2}\right)^2 + \left(\frac{e_c}{c}\right)^2\right]} \tag{42}$$

$$V_\alpha = \frac{\frac{k}{16}\left(1+32\frac{e_m^2}{c^2}\right)\left(G_m - \frac{\bar{e}}{c}G_c\right) + \frac{e_c}{c}\left(F_m - \frac{\bar{e}}{c}F_c\right)}{\pi k\alpha_0\left[\left(\frac{k}{16}\right)^2\left(1+32\frac{e_m^2}{c^2}\right)^2 + \left(\frac{e_c}{c}\right)^2\right]} \tag{43}$$

III. Transonic Correction for Oscillating Airfoil in Plunge

The motion of an airfoil in plunge is related to the pitching motion by the effective angle of attack

$$\alpha_{eff} = \frac{\dot{h}}{V_\infty} \tag{44}$$

To establish the equivalent angle of the attack, the plunging motion is described by

$$h = -h_0 \cos \omega t = -h_0 \cos k\tau \tag{45}$$

Then, the airfoil sees an angle of attack

$$\alpha = \bar{\alpha} + \frac{\dot{h}}{V_\infty} = \bar{\alpha} + \frac{2h_0 k}{c} \sin k\tau \tag{46}$$

To establish the equivalent angle of attack, the plunging motion is prescribed by setting $\alpha_0 = \frac{2h_0 k}{c}$.

A. Unsteady Lift Transonic Correction

Applying the transonic correction, the unsteady lift coefficient for the plunging motion is expressed as

$$\begin{aligned} \tilde{c}_l &= (U_h + iW_h)\, c_{l_\alpha} \left[C(k) \frac{2}{c} \frac{dh}{d\tau} + \frac{1}{c} \frac{d^2 h}{d\tau^2} \right] \\ &= c_{l_\alpha} \alpha_0 \left[FU_h - \left(G + \frac{k}{2} \right) W_h \right] \sin k\tau + c_{l_\alpha} \alpha_0 \left[\left(G + \frac{k}{2} \right) U_h + FW_h \right] \cos k\tau \end{aligned} \tag{47}$$

The Fourier sine and cosine transforms of the unsteady lift coefficient are computed as

$$\int_0^{\frac{2n\pi}{k}} \tilde{c}_l \sin k\tau d\tau = \frac{n\pi}{k} c_{l_\alpha} \alpha_0 \left[FU_h - \left(G + \frac{k}{2} \right) W_h \right] \tag{48}$$

$$\int_0^{\frac{2n\pi}{k}} \tilde{c}_l \cos k\tau d\tau = \frac{n\pi}{k} c_{l_\alpha} \alpha_0 \left[\left(G + \frac{k}{2} \right) U_h + FW_h \right] \tag{49}$$

Thus, the correction functions U_h and W_h are obtained as

$$U_h = \frac{k \left[F \int_0^{\frac{2n\pi}{k}} \tilde{c}_l \sin k\tau d\tau + \left(G + \frac{k}{2} \right) \int_0^{\frac{2n\pi}{k}} \tilde{c}_l \cos k\tau d\tau \right]}{n\pi c_{l_\alpha} \alpha_0 \left[F^2 + \left(G + \frac{k}{2} \right)^2 \right]} \tag{50}$$

$$W_h = \frac{k \left[F_k \int_0^{\frac{2n\pi}{k}} \tilde{c}_l \cos k\tau d\tau - \left(G + \frac{k}{2} \right) \int_0^{\frac{2n\pi}{k}} \tilde{c}_l \sin k\tau d\tau \right]}{n\pi c_{l_\alpha} \alpha_0 \left[F^2 + \left(G + \frac{k}{2} \right)^2 \right]} \tag{51}$$

B. Unsteady Pitching Moment Transonic Correction

The unsteady pitching moment coefficient for the plunging motion can be corrected as

$$\tilde{c}_m = \left[\frac{\bar{e}}{c} - (A_h + iB_h) \frac{1}{h_0 k} \frac{dh}{d\tau} \right] (U_h + iW_h)\, c_{l_\alpha} C(k) \frac{2}{c} \frac{dh}{d\tau} - (T_h + iV_h)\, 2\pi \frac{e_m}{c} \frac{1}{c} \frac{d^2 h}{d\tau^2} \tag{52}$$

The expression for the unsteady pitching moment coefficient is expanded as

$$\begin{aligned}\tilde{c}_m &= \left[\frac{\bar{e}}{c} - (A_h + iB_h)\sin k\tau\right]\left[c_{l_\alpha}\alpha_0 (FU_h - GW_h)\sin k\tau + c_{l_\alpha}\alpha_0 (FW_h + GU_h)\cos k\tau\right] \\ &\quad - (T_h + iV_h)\, 2\pi \frac{e_m}{c}\frac{1}{c}\frac{d^2h}{d\tau^2} \\ &= \left(\frac{\bar{e}}{c}F_h + \pi k\alpha_0\frac{e_m}{c}V_h\right)\sin k\tau + \left(\frac{\bar{e}}{c}G_h - \pi k\alpha_0\frac{e_m}{c}T_h\right)\cos k\tau \\ &\quad - \frac{1}{2}(F_hA_h - G_hB_h) + \frac{1}{2}(F_hA_h - G_hB_h)\cos 2k\tau - \frac{1}{2}(G_hA_h + F_hB_h)\sin 2k\tau \end{aligned} \tag{53}$$

where

$$F_h = c_{l_\alpha}\alpha_0 (FU_h - GW_h) \tag{54}$$

$$G_h = c_{l_\alpha}\alpha_0 (GU_h + FW_h) \tag{55}$$

The Fourier sine and cosine transforms of the unsteady pitching coefficient are computed as

$$\int_0^{\frac{2n\pi}{k}} \tilde{c}_m \sin k\tau d\tau = \frac{n\pi}{k}\left(\frac{\bar{e}}{c}F_h + \pi k\alpha_0\frac{e_m}{c}V_h\right) \tag{56}$$

$$\int_0^{\frac{2n\pi}{k}} \tilde{c}_m \cos k\tau d\tau = \frac{n\pi}{k}\left(\frac{\bar{e}}{c}G_h - \pi k\alpha_0\frac{e_m}{c}T_h\right) \tag{57}$$

$$\int_0^{\frac{2n\pi}{k}} \tilde{c}_m \sin 2k\tau d\tau = -\frac{n\pi}{2k}(G_hA_h + F_hB_h) \tag{58}$$

$$\int_0^{\frac{2n\pi}{k}} \tilde{c}_m \cos 2k\tau d\tau = \frac{n\pi}{2k}(F_hA_h - G_hB_h) \tag{59}$$

Thus, we obtain the transonic correction functions A_h, B_h, T_h, and V_h as

$$A_h = \frac{2k\left(F_h\int_0^{\frac{2n\pi}{k}} \tilde{c}_m \cos 2k\tau d\tau - G_h\int_0^{\frac{2n\pi}{k}} \tilde{c}_m \sin 2k\tau d\tau\right)}{n\pi\left(F_h^2 + G_h^2\right)} \tag{60}$$

$$B_h = -\frac{2k\left(F_h\int_0^{\frac{2n\pi}{k}} \tilde{c}_m \sin 2k\tau d\tau + G_h\int_0^{\frac{2n\pi}{k}} \tilde{c}_m \cos 2k\tau d\tau\right)}{n\pi\left(F_h^2 + G_h^2\right)} \tag{61}$$

$$T_h = \frac{-\frac{k}{n\pi}\int_0^{\frac{2n\pi}{k}} \tilde{c}_m \cos k\tau d\tau + \frac{\bar{e}}{c}G_h}{\pi k\alpha_0\frac{e_m}{c}} \tag{62}$$

$$V_h = \frac{\frac{k}{n\pi}\int_0^{\frac{2n\pi}{k}} \tilde{c}_m \sin k\tau d\tau - \frac{\bar{e}}{c}F_h}{\pi k\alpha_0\frac{e_m}{c}} \tag{63}$$

IV. Simulations

A series of unsteady RANS simulations of oscillating transonic airfoils are conducted in FUN3D. The airfoils being studied are extracted from the Boeing Transonic Truss-Braced Wing (TTBW) aircraft configuration developed for Mach 0.745.[5,6] The data presented in this section is obtained from the TTBW airfoil at the mean aerodynamic chord (MAC). Data for three other airfoil stations are also available for additional analyses. Steady-state simulations in FUN3D are conducted for Mach 0.6, 0.7, 0.8 at the angles of attack of -1.5°, -1°, -0.5°, and 0° to obtain the lift curve slope c_{l_α} for the unsteady transonic correction analysis. To better understand this behavior, FUN3D steady-state simulations are conducted over a wider range of Mach number from 0.6 to 1 at an increment of 0.1 which also includes Mach 0.745 and a wider range of the angle of attack from -2° to 1° at an increment of 0.5°.

A. Steady-State Simulations

Figures 1(a) and (b) show the plots of the lift coefficient of the MAC airfoil computed by FUN3D as a function of the angle of attack for various Mach numbers and the lift curve slope as a function of Mach number at various angles of attack, respectively. The lift curve at Mach 0.745 is nonlinear for angles of attack greater than zero. This is likely due to stall as the flow begins to separate at the trailing edge. The lift curve at Mach 0.8 is entirely nonlinear over the angle of attack range. The lift coefficient decreases precipitously above Mach 0.745. The lift curves at Mach 0.9 and 1 are generally linear.

The lift curve slope is computed by cubic spline curvefitting of the FUN3D results. It can be seen that the lift curve slope is strongly dependent on the angle of attack as shown in Fig. 1(b). The lift curve slope has a maximum value at Mach 0.745 and the angle of attack of -2° and decreases rapidly to a minimum value at Mach 0.745 and the angle of attack of 1°.

It should be noted that the CFD simulations do not take into account the wing sweep which acts to reduce the effective Mach number by the factor of $\cos\Lambda$ where Λ is the sweep angle of the mid-chord at the MAC wing station. So the Mach number in the simulations should be interpreted as the effective Mach number that the airfoil sees. The corresponding free-stream Mach number is higher than the indicated Mach number by the factor of $1/\cos\Lambda$.

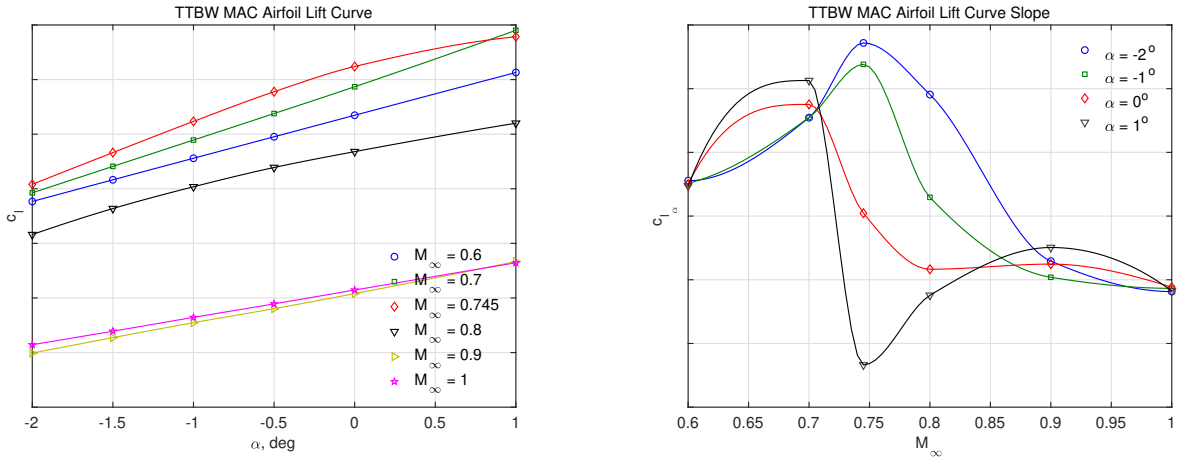

(a) (b)

Figure 1. TTBW MAC Airfoil c_l vs. α and c_{l_α} vs. M_∞

Figures 2(a) and (b) show the computed pitching moment curve slope and the steady-state aerodynamic center as a fraction of chord as functions of the Mach number, respectively. As the Mach number increases, the aerodynamic center moves from about the quarter-chord location to the mid-chord location. This is seen in Fig. 2(b). The pitching moment curve slope correspondingly decreases as the Mach number increases as shown in Fig. 2(a). A break from the trend in both curves occurs at Mach 0.745.

Figure 3 shows the velocity contour of the TTBW MAC airfoil, which is illustrated by a NASA supercritical airfoil as a substitute for the exact TTBW MAC airfoil which cannot be shown, at various angles of attack for Mach 0.8. At the angle of attack of -2°, there is an accelerating supersonic flow region on the lower surface toward the leading edge while the flow on the upper surface reaches supersonic further downstream from the leading edge. There is a retarded flow region on the lower surface where the flow could be separated due to the shock-boundary layer interaction. The supersonic flow on the lower surface is the likely cause of the decrease in lift at Mach 0.8. As the angle of attack increases, the accelerating flow region on the lower surface diminishes and the flow becomes entirely subsonic at zero angle of attack. As the angle of attack increases above zero, the shock becomes steeper and the shock-boundary layer interaction causes an increase in the retarded flow region aft of the shock due to the shock-boundary layer interaction. This could be a plausible explanation for the nonlinear behavior of the lift curve at Mach 0.8.

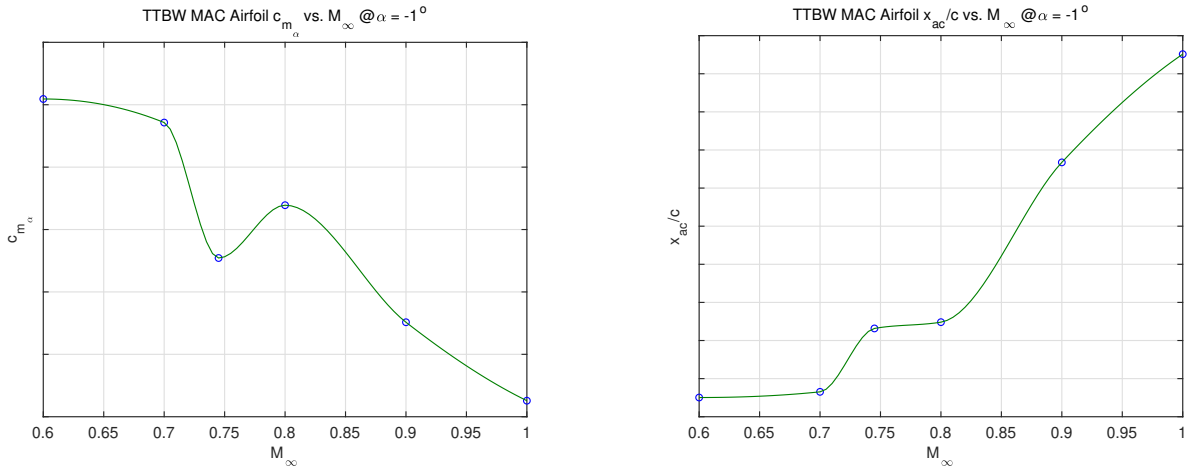

(a) (b)

Figure 2. TTBW MAC Airfoil c_{m_α} vs. M_∞ and $\frac{x_{ac}}{c}$ vs. M_∞

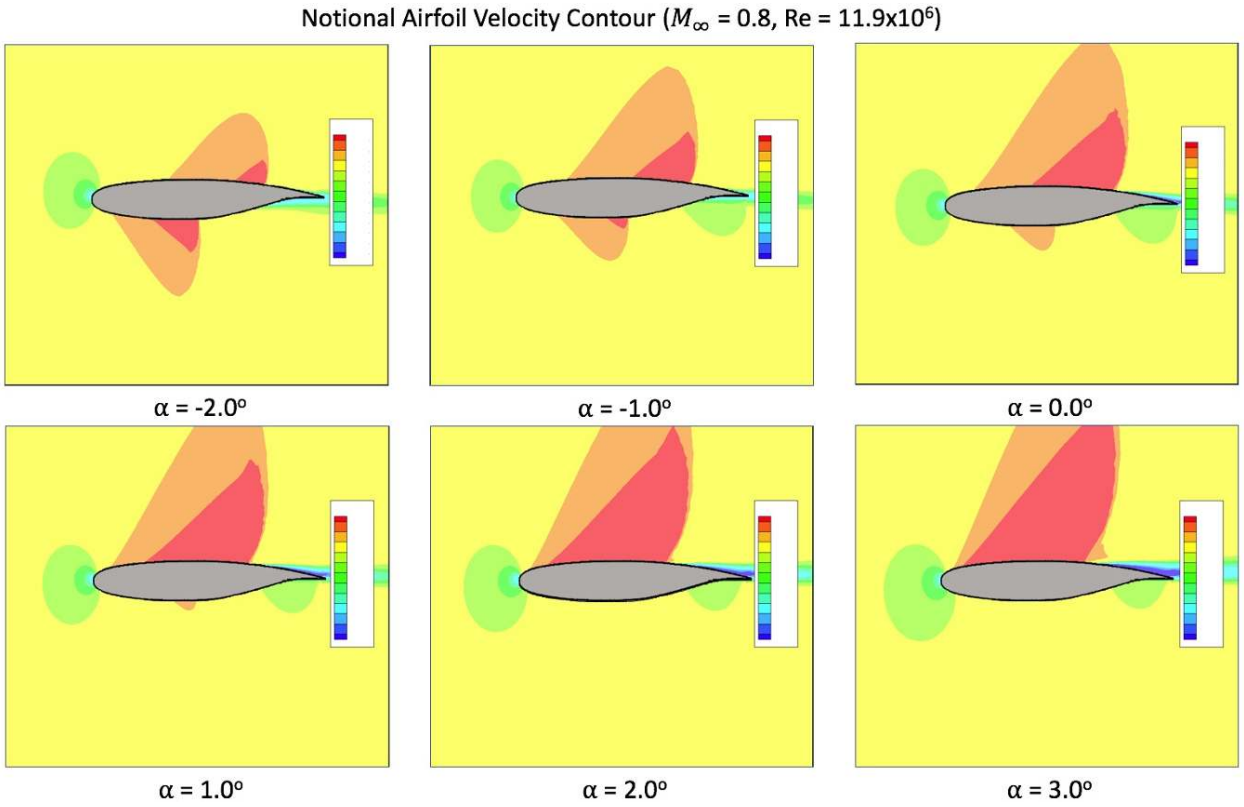

Figure 3. Notional Airfoil Velocity Contour at Mach 0.8 Computed by FUN3D

B. Unsteady Simulations of Oscillating Airfoil in Pitch

Unsteady simulations of the MAC airfoil oscillating about the quarter-chord location are conducted in FUN3D for Mach 0.6, 0.7, and 0.8 at Reynolds numbers corresponding to an altitude of 40,000 ft based on the local chord and four different reduced frequencies $k = 0.02$, 0.1, 0.2, and 0.3. The FUN3D mesh has about 30 thousand grid points. The mesh domain size is about 100 times the airfoil chord length. The Roe's flux-difference splitting scheme and the

Spalart-Allmaras turbulence model are used in the simulations. An optimized second-order backward finite-difference scheme is used in the time integration. To minimize nonlinear aerodynamic effects as seen in the steady-state results, the harmonic angle of attack is chosen with $\bar{\alpha} = -1^\circ$ and $\alpha_0 = 0.5^\circ$. So, the angle of attack oscillates between -1.5° and -0.5°. Within this angle of attack range, the steady-state lift coefficients at Mach 0.6 and 0.7 are linear, but the steady-state lift coefficient at Mach 0.8 is nonlinear. The unsteady transonic correction method is applied to the unsteady lift and pitching moment coefficients computed by FUN3D.

Selected figures from the analysis are presented to illustrate the method. Figures 4(a) and (b) are the plots of the unsteady lift coefficient computed by FUN3D for Mach 0.8 and the reduced frequency $k = 0.02$ as a function of time and as a function of the angle of attack, respectively. The computed unsteady lift coefficient by the transonic correction method is in good agreement with the FUN3D results.

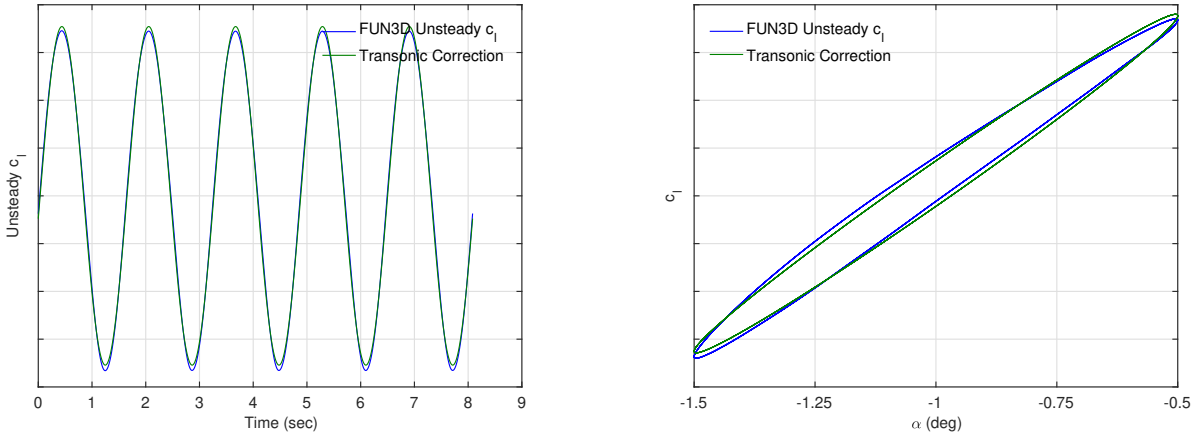

(a) (b)

Figure 4. TTBW MAC Airfoil c_l Time History and c_l vs. α for Mach 0.8, $k = 0.02$, $\bar{\alpha} = -1^\circ$, and $\alpha_0 = 0.5^\circ$

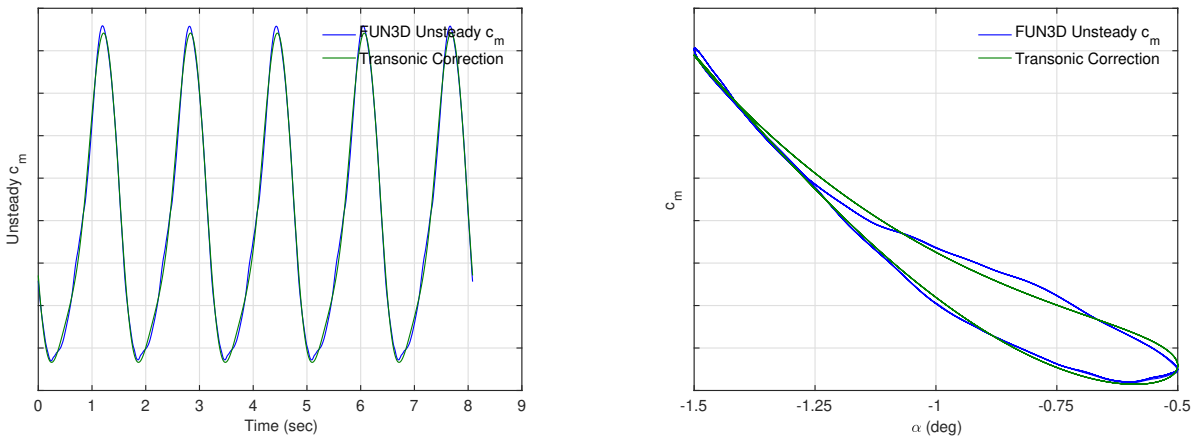

(a) (b)

Figure 5. TTBW MAC Airfoil c_m Time History and c_m vs. α for Mach 0.8, $k = 0.02$, $\bar{\alpha} = -1^\circ$, and $\alpha_0 = 0.5^\circ$

Figures 5(a) and (b) present the plots of the unsteady pitching moment coefficient for Mach 0.8 and the reduced frequency $k = 0.02$ as a function of time and as a function of the angle of attack, respectively. The unsteady pitching moment coefficient exhibits a strong nonlinearity not seen in the unsteady lift coefficient in Figures 4(a) and (b). The transonic correction method is able to capture the nonlinear pitching moment coefficient quite accurately. An excellent agreement is demonstrated in the time histories of the unsteady pitching moment coefficients between the

FUN3D results and the transonic correction. The hysteresis loop between the unsteady pitching moment and the angle of attack illustrates the strong nonlinearity in Fig. 5(b). The match in the hysteresis loop is generally quite good.

The nonlinear effect in the unsteady pitching moment coefficient is postulated to be due to the unsteady motion of the aerodynamic center resulting from the moving shock. The inclusion of the term that captures the unsteady motion of the aerodynamic center in the transonic correction method enables the unsteady pitching moment coefficient to be accurately modeled. Figures 6(a) and (b) present the plots of the unsteady aerodynamic center about the steady-state aerodynamic center for Mach 0.8 and the reduced frequency $k = 0.02$ as a function of time and as a function of the angle of attack, respectively. The motion is about 2.3% of chord.

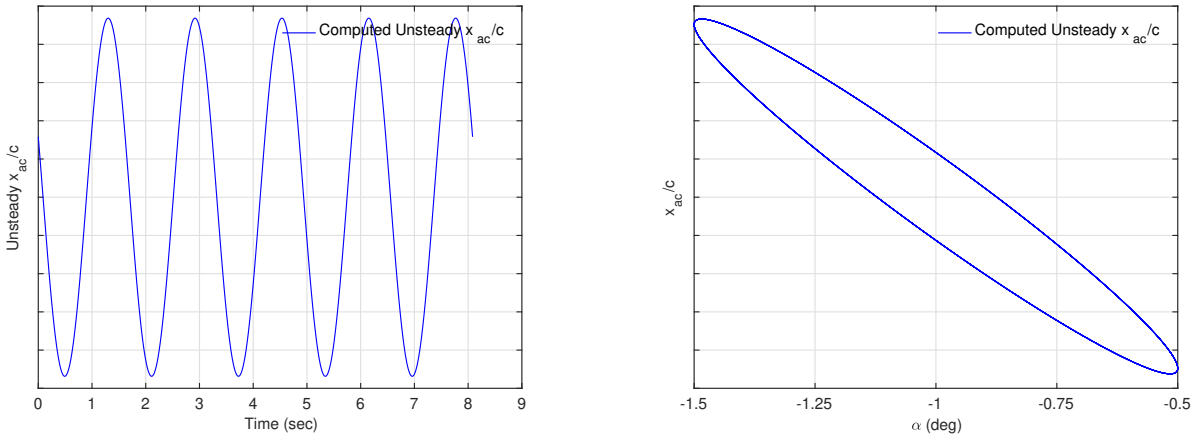

(a) (b)

Figure 6. TTBW MAC Airfoil x_{ac} Time History and x_{ac} vs. α for Mach 0.8, $k = 0.02$, $\bar{\alpha} = -1°$, and $\alpha_0 = 0.5°$

To illustrate the effect of the reduced frequency, Figures 7(a) and (b) present the plots of the unsteady lift coefficient for Mach 0.8 and the reduced frequency $k = 0.3$ as a function of time and as a function of the angle of attack, respectively. The transonic correction method captures the unsteady lift coefficient very accurately.

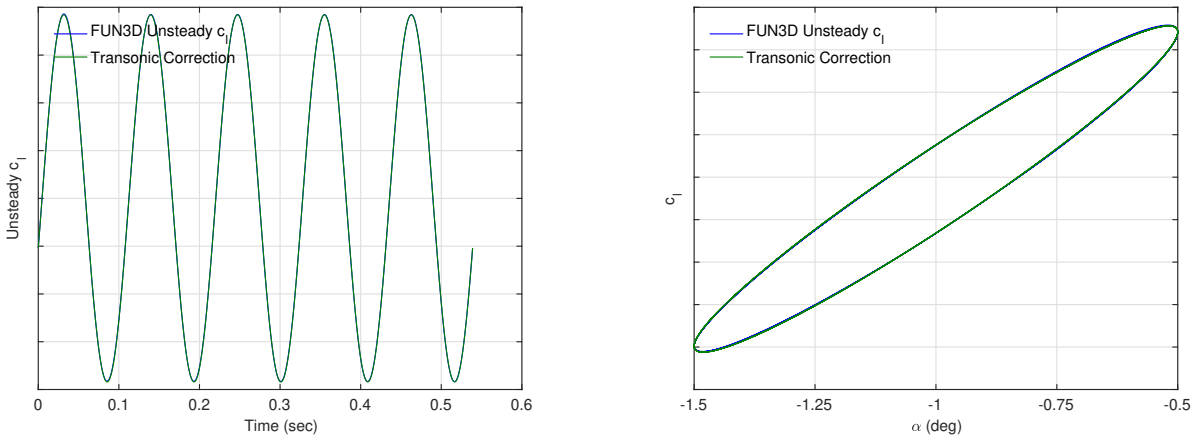

(a) (b)

Figure 7. TTBW MAC Airfoil c_l Time History and c_l vs. α for Mach 0.8, $k = 0.3$, $\bar{\alpha} = -1°$, and $\alpha_0 = 0.5°$

Figures 8(a) and (b) show the plots of the unsteady pitching moment coefficient for Mach 0.8 and the reduced frequency $k = 0.3$ as a function of time and as a function of the angle of attack, respectively. It is interesting to note that the strong nonlinearity in the unsteady pitching moment coefficient for the reduced frequency $k = 0.02$ is not present in the unsteady pitching moment for the reduced frequency $k = 0.3$. Nonetheless, the hysteresis loop between

the unsteady pitching moment and the angle of attack indicates a slight nonlinearity in the unsteady pitching moment coefficient. A possible explanation for the reduced nonlinearity in the unsteady pitching moment coefficient as the reduced frequency increases could be due to the lift circulation not being able to fully establish at higher values of the reduced frequency. At very small values of the reduced frequency, the flow is dominated by the steady-state lift circulation which is strongly nonlinear in transonic flow. Therefore, as the flow begins to transition from a steady flow to unsteady flow, the nonlinear effect of the steady flow may still dominate.

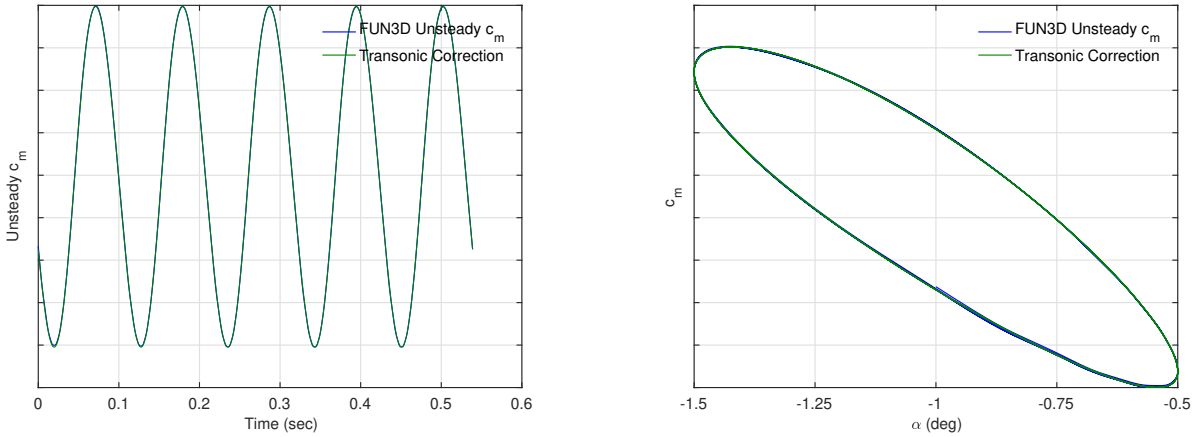

(a) (b)

Figure 8. TTBW MAC Airfoil c_m Time History and c_m vs. α for Mach 0.8, $k = 0.3$, $\bar{\alpha} = -1^\circ$, and $\alpha_0 = 0.5^\circ$

Figures 9(a) and (b) show the plots of the unsteady aerodynamic center computed by the transonic correction method for Mach 0.8 and the reduced frequency $k = 0.3$ as a function of time and as a function of the angle of attack, respectively. The motion of the aerodynamic center is about 0.8% of chord. It is noted that the amplitude of the motion of the aerodynamic center decreases as the reduced frequency increases when comparing Fig. 6 to Fig. 9. It is also interesting to note that the phase angle of the motion of the aerodynamic center reverses.

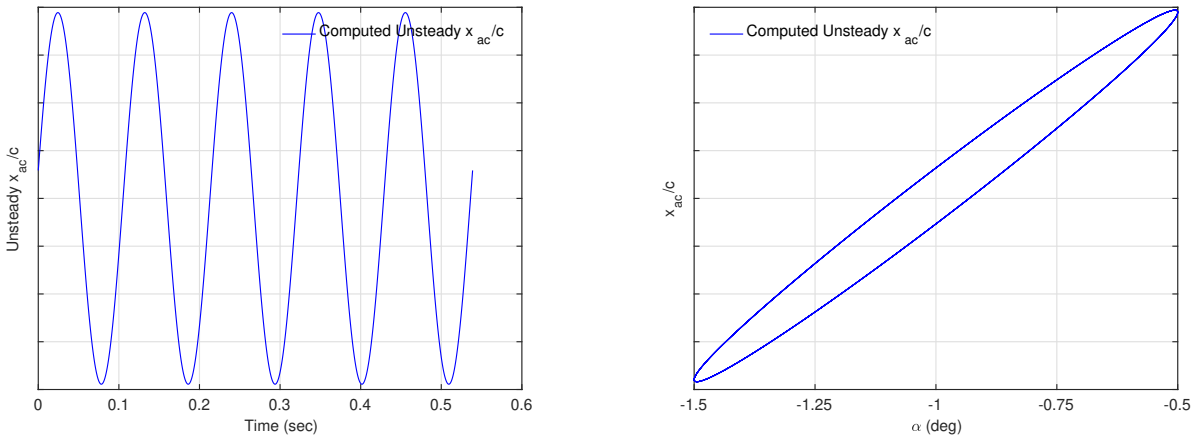

(a) (b)

Figure 9. TTBW MAC Airfoil x_{ac} Time History and x_{ac} vs. α for Mach 0.8, $k = 0.3$, $\bar{\alpha} = -1^\circ$, and $\alpha_0 = 0.5^\circ$

To further illustrate the effect of the reduced frequency on the motion of the aerodynamic center, Fig. 10(a) and (b) show the pressure coefficients for the reduced frequency $k = 0.02$ and $k = 0.3$ corresponding to the aftmost shock position and mean shock position for Mach 0.8, the mean angle of attack of -1°, and the amplitude of oscillation of 0.5°. Shocks exist on both upper and lower surfaces, but the upper surface shock dominates as it causes the pressure

center to shift aft. The shock movement can be seen on the surface pressure coefficient plots. The displacement of the upper surface shock position is greater for the reduced frequency $k = 0.02$ than for the reduced frequency $k = 0.3$. The displacement is estimated to be about 1.6% for the reduced frequency $k = 0.02$ and 0.8% for the reduced frequency $k = 0.3$. These estimates are close to the estimates computed from the transonic correction method. This observation thus supports the postulate of the motion of the aerodynamic center.

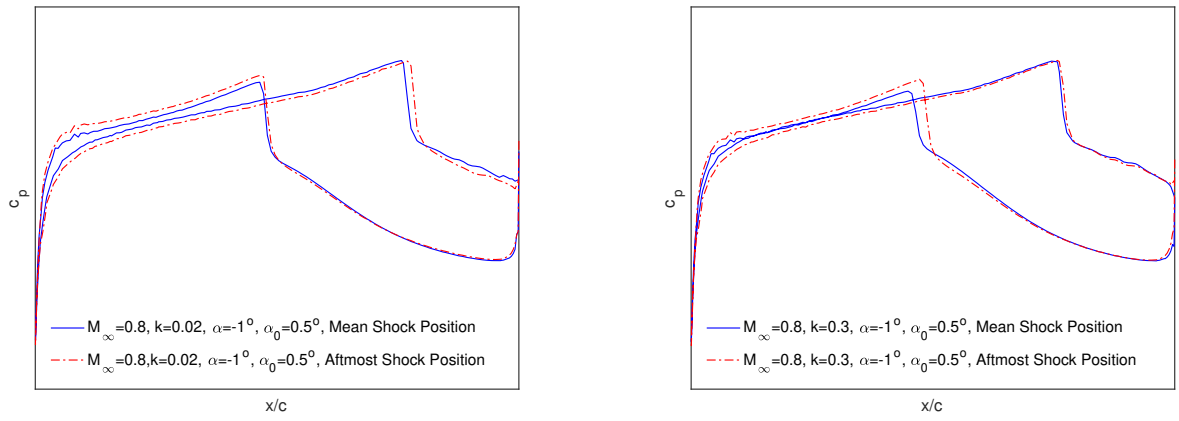

(a) (b)

Figure 10. TTBW MAC Airfoil c_p for Mach 0.8, $k = 0.02$ and $k = 0.3$, $\bar{\alpha} = -1^\circ$, and $\alpha_0 = 0.5^\circ$

Figures 11(a) and (b) present the plots of the amplitude and phase correction functions U_α and W_α for the unsteady lift coefficient, respectively. The functions vary with the Mach number and the reduced frequency for the amplitude of oscillation of 0.5°. The amplitude correction function U_α shows a decrease in the amplitude as the reduced frequency increases at a given Mach number. The phase correction function W_α also shows an increase in the phase lag as the reduced frequency increases.

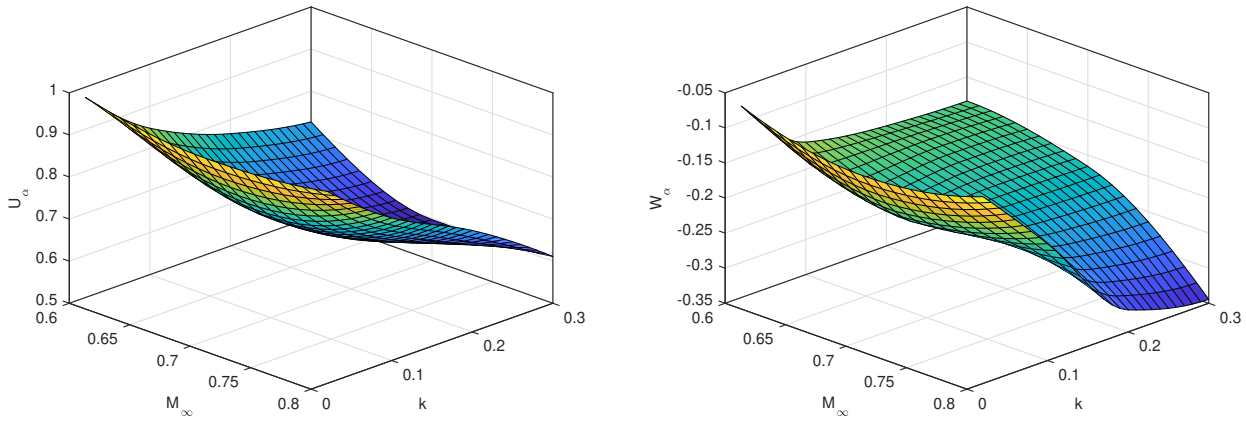

(a) (b)

Figure 11. TTBW MAC Airfoil Transonic Correction Functions U_α and W_α for Unsteady Lift for $\bar{\alpha} = -1^\circ$ and $\alpha_0 = 0.5^\circ$

Figures 12(a) and (b) present the plots of the functions A_α and B_α that model the motion of the aerodynamic center, respectively. The function A_α represents the amplitude of the motion of the aerodynamic center and clearly shows an increased amplitude at Mach 0.8 and $k = 0.02$. As the reduced frequency increases, the amplitude of the motion tends to decrease. The function B_α represents the phase angle relative to the motion of the angle of attack. As the reduced frequency increases, the phase angle decreases.

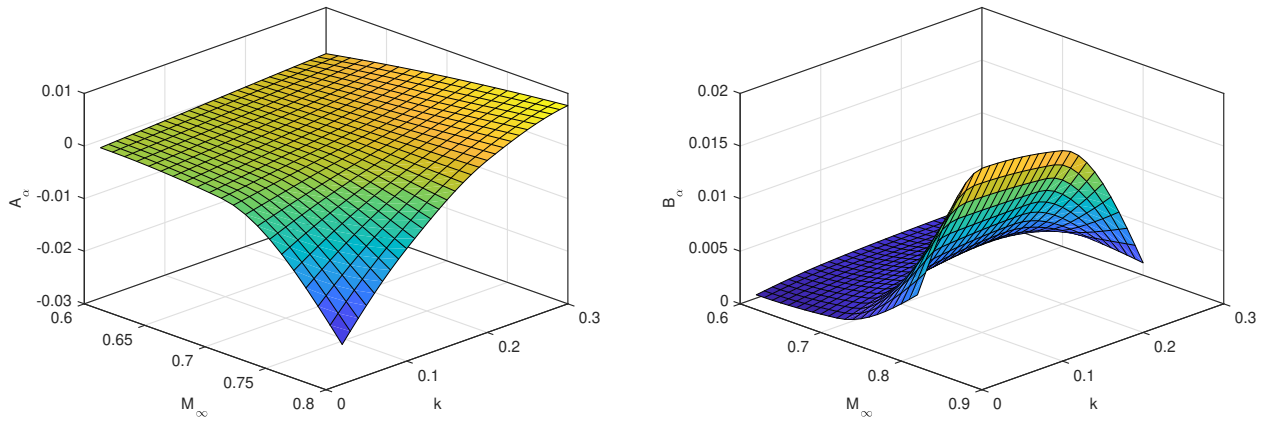

(a) (b)

Figure 12. TTBW MAC Airfoil Transonic Correction Functions A_α and B_α for Aerodynamic Center Motion for $\bar{\alpha} = -1^\circ$ and $\alpha_0 = 0.5^\circ$

Figures 13(a) and (b) show the plots of the functions T_α and V_α that correct for the amplitude and phase angle of the non-circulatory pitching moment coefficient. The functions show increased negative values at Mach 0.8 and $k = 0.02$ which indicate an increased correction for the non-circulatory pitching moment coefficient due to the nonlinear effect.

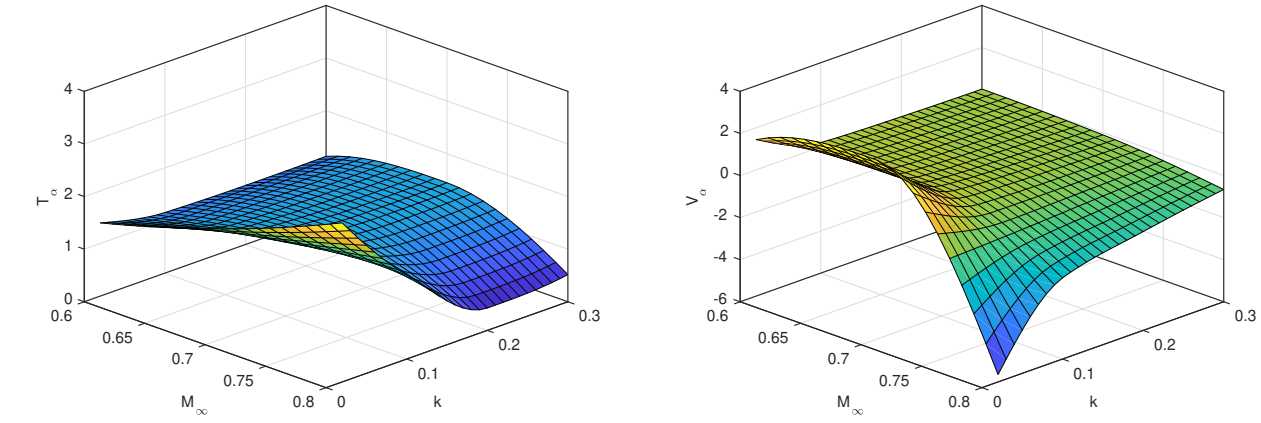

(a) (b)

Figure 13. TTBW MAC Airfoil Transonic Correction Functions T_α and V_α for Non-Circulatory Pitching Moment for $\bar{\alpha} = -1^\circ$ and $\alpha_0 = 0.5^\circ$

The effect of the amplitude of oscillation is examined next. The data for the amplitude of oscillation $\alpha_0 = 0.5^\circ$ are compared to the data for $\alpha_0 = 0.1^\circ$ at the same mean angle of attack $\bar{\alpha} = -1^\circ$ and Mach number. In addition, the effect of the mean angle of attack is also examined. The data for different mean angles of attack for Mach 0.6 and 0.7 at the same amplitude of oscillation of $\alpha_0 = 0.1^\circ$ are also compared. Figures 14(a) and (b) show the plots of the amplitude correction function U_α and phase correction function W_α for the unsteady lift versus the reduced frequency, respectively. The effect of the amplitude of oscillation appears to be small for Mach 0.6 and 0.7 as the plots for the two sets of data for $\alpha_0 = 0.5^\circ$ and $\alpha_0 = 0.1^\circ$ are virtually on top of each other. A small difference is noted for Mach 0.8 at the reduced frequency greater than $k = 0.25$. The data for Mach 0.6 and Mach 0.7 indicate a trend of decreasing the amplitude and increasing the phase angle with increasing the Mach number. However, the data for Mach 0.8 does not follow this trend. It should be noted that the flow at Mach 0.8 is nonlinear. The effect of the mean angle of attack can be observed in the data for Mach 0.6 at $\bar{\alpha} = -1^\circ$ and $\bar{\alpha} = -0.80^\circ$ and for Mach 0.7 at $\bar{\alpha} = -1^\circ$ and $\bar{\alpha} = 0.23^\circ$. The effect is small but noticeable for Mach 0.6 and 0.7. The effect of the mean angle of attack for Mach 0.8 is large

but the data is not plotted for better clarity.

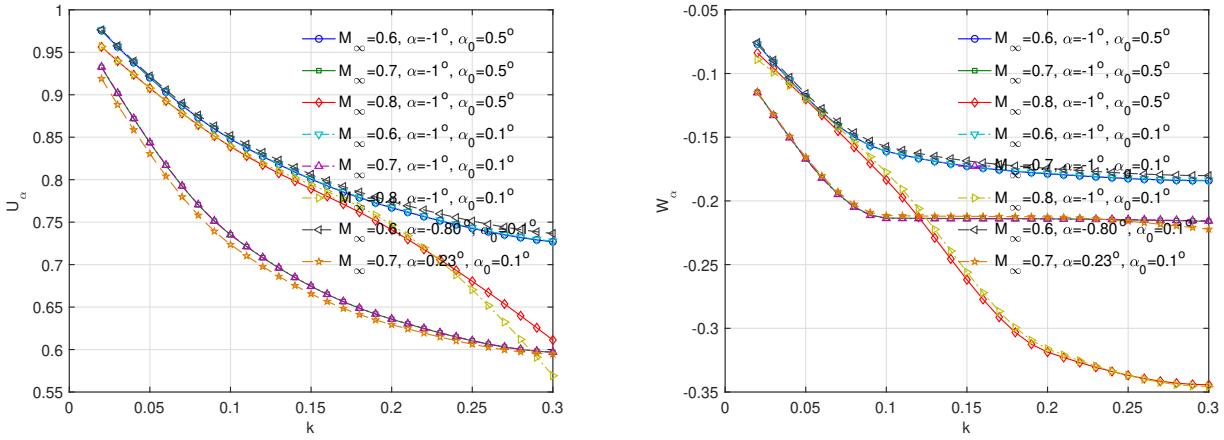

(a) (b)

Figure 14. TTBW MAC Airfoil Transonic Correction Functions U_α and W_α for Unsteady Lift versus Reduced Frequency

Figures 15(a) and (b) show the plots of the transonic correction functions A_α and B_α for the aerodynamic center motion versus the reduced frequency, respectively. These transonic correction functions contribute to the nonlinearity of the unsteady pitching moment coefficient. Except for Mach 0.8, their values are generally small for Mach 0.6 and Mach 0.7. Increasing the amplitude of oscillation causes the motion of the aerodynamic center to increase.

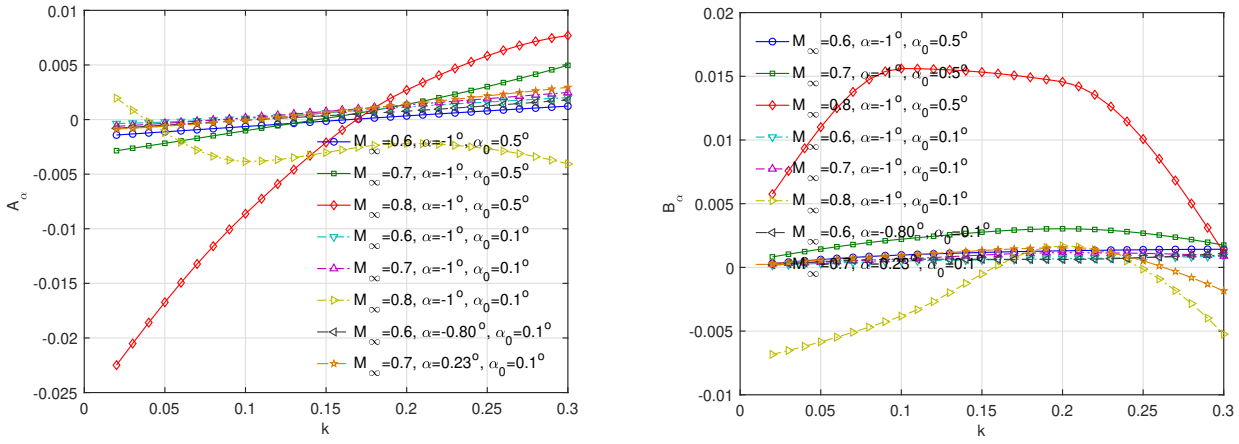

(a) (b)

Figure 15. TTBW MAC Airfoil Transonic Correction Functions A_α and B_α for Aerodynamic Center Motion versus Reduced Frequency

Figures 16(a) and (b) show the plots of the amplitude correction function T_α and phase correction function V_α for the non-circulatory pitching moment versus the reduced frequency, respectively. The data seem to suggest an asymptotic behavior for the transonic correction functions T_α and V_α. As the reduced frequency increases, the values of T_α tend to constant values and the values of V_α tend to converge to zero. The effects of the amplitude of oscillation and the mean angle of attack are generally small for Mach 0.6 and Mach 0.7.

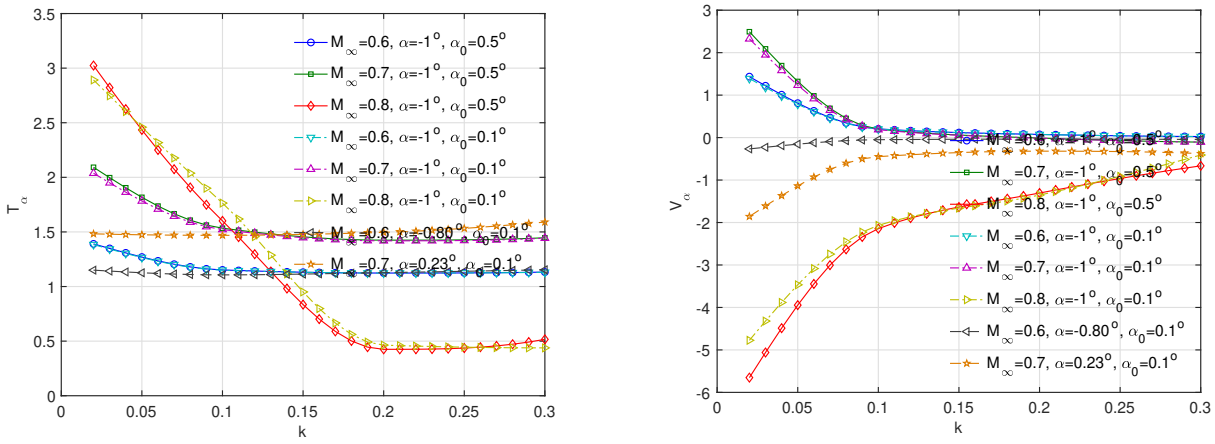

(a) (b)

Figure 16. TTBW MAC Airfoil Transonic Correction Functions T_α and V_α for Non-Circulatory Pitching Moment versus Reduced Frequency

C. Unsteady Simulations of Oscillating Airfoil in Plunge

A FUN3D CFD simulation of the TTBW MAC airfoil in plunge is conducted for Mach 0.65, Mach 0.7, and Mach 0.75 at the reduced frequency of $k = 0.1$ and an equivalent amplitude of oscillation of $\alpha_0 = \frac{2h_0 k}{c} = 0.1^\circ$. The mean angle of attack is varying at $\bar{\alpha} = 0.41^\circ$ for Mach 0.65, $\bar{\alpha} = 0.08^\circ$ for Mach 0.7, and $\bar{\alpha} = -0.23^\circ$. These mean angles of attack are chosen to match the section lift coefficient on the full configuration of the TTBW at the design lift coefficient of 0.73 which is computed from steady-state FUN3D simulations of the full vehicle as shown in Fig. 17.

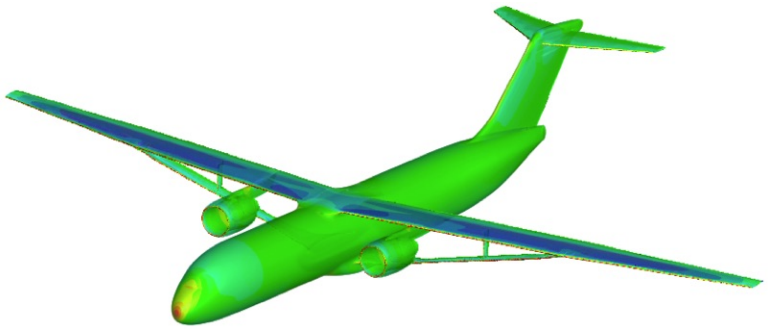

Figure 17. FUN3D C_p Contour of the Mach 0.745 TTBW at Design $C_L = 0.73$

Figures 18(a) and (b) show the plots of the unsteady lift coefficient of the MAC airfoil in pitch and plunge for Mach 0.75 and the reduced frequency $k = 0.1$ as a function of time and as a function of the angle of attack, respectively. The lift coefficients in pitch and plunge have essentially the same amplitudes but the lift coefficient in plunge lags the lift coefficient in pitch by $\Delta\tau = 0.78$.

Figures 19(a) and (b) show the plots of the unsteady pitching moment coefficient of the MAC airfoil in pitch and plunge for Mach 0.75 and the reduced frequency $k = 0.1$ as a function of time and as a function of the angle of attack, respectively. The pitching moment coefficients in pitch and plunge have almost the same amplitudes but the lift coefficient in plunge lags the lift coefficient in pitch by $\Delta\tau = 2.39$. The nonlinear effect can be seen in the non-elliptical hysteresis loop between the unsteady pitching moment and the angle of attack.

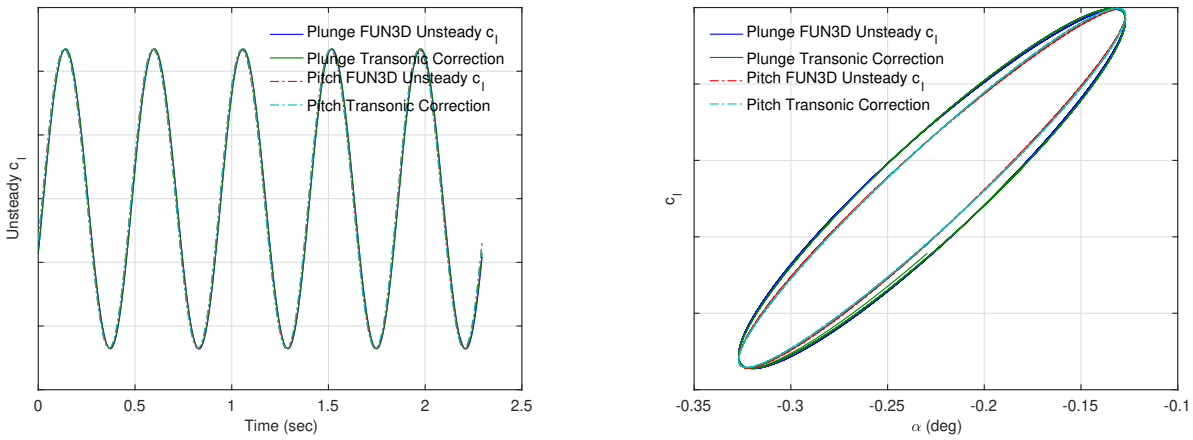

(a) (b)

Figure 18. TTBW MAC Airfoil c_l Time History and c_l vs. α for Mach 0.75, $k = 0.1$, $\bar{\alpha} = -0.23°$, and $\alpha_0 = \frac{2h_0k}{c} = 0.1°$

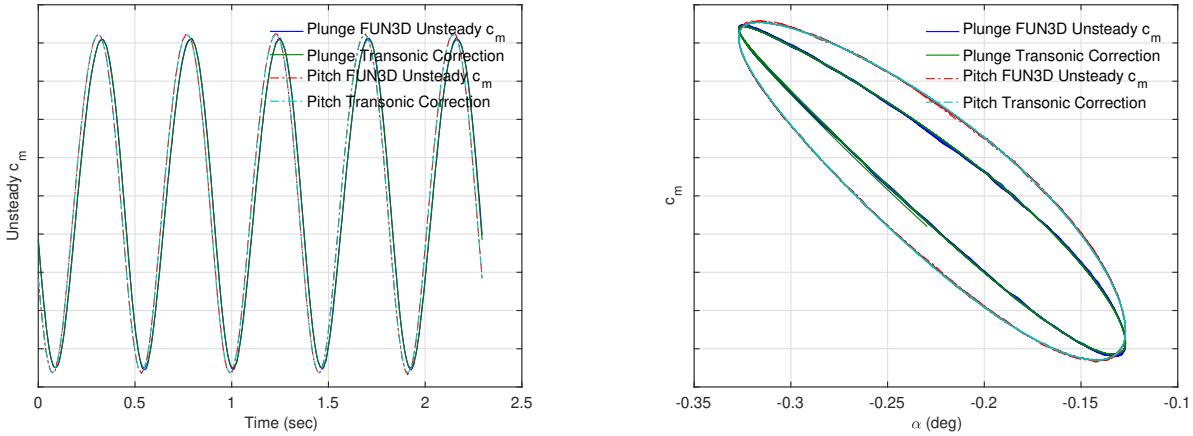

(a) (b)

Figure 19. TTBW MAC Airfoil c_m Time History and c_m vs. α for Mach 0.75, $k = 0.1$, $\bar{\alpha} = -0.23°$, and $\alpha_0 = \frac{2h_0k}{c} = 0.1°$

Figures 20(a) and (b) show the plots of the unsteady aerodynamic center of the MAC airfoil in pitch and plunge for Mach 0.75 and the reduced frequency $k = 0.1$ as a function of time and as a function of the angle of attack, respectively. The plunging motion produces a slightly greater motion of the aerodynamic center than the pitching motion. The unsteady aerodynamic center in plunge lags the unsteady aerodynamic center in pitch by $\Delta\tau = 1.38$.

Figures 21(a) and (b) show the plots of the amplitude correction function U_h and phase correction function W_h for the unsteady lift versus the Mach number, respectively. The amplitude correction function U_h is slightly larger for the plunging motion than for the pitching motion by an almost constant offset. The phase correction function W_h is smaller in amplitude for the plunging motion than for the pitching motion. The phase correction greatly increases for Mach 0.75.

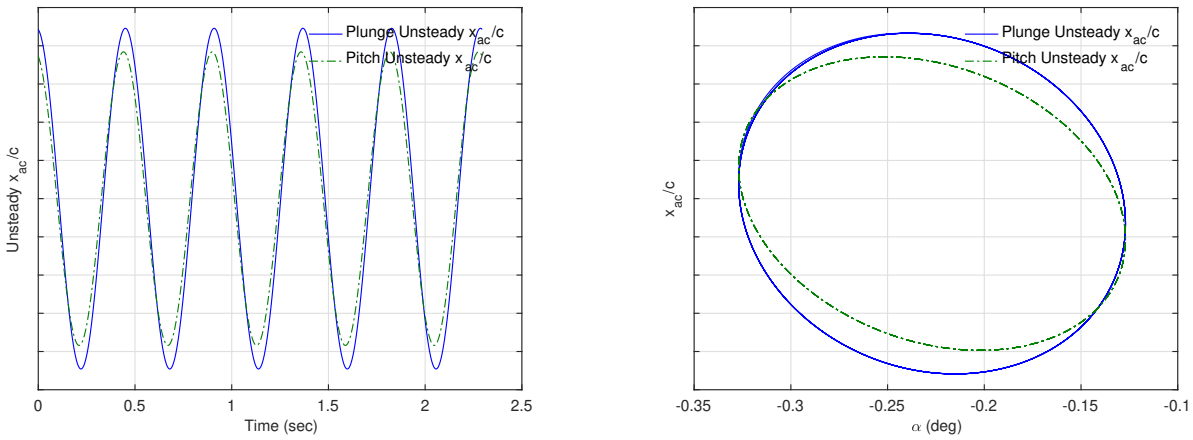

(a) (b)

Figure 20. TTBW MAC Airfoil x_{ac} Time History and x_{ac} vs. α for Mach 0.75, $k = 0.1$, $\bar{\alpha} = -0.23°$, and $\alpha_0 = \frac{2h_0 k}{c} = 0.1°$

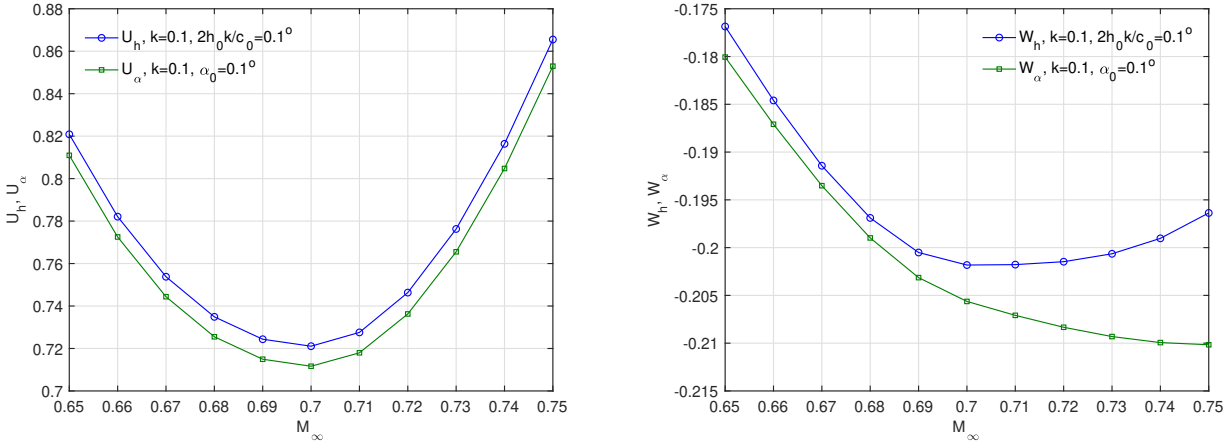

(a) (b)

Figure 21. TTBW MAC Airfoil Transonic Correction Functions U_h and W_h for Unsteady Lift versus Mach Number for $k = 0.1$ and $\alpha_0 = \frac{2h_0 k}{c} = 0.1°$

Figures 22(a) and (b) show the plots of the correction functions A_h and B_h for the aerodynamic center motion versus the Mach number, respectively. These transonic correction functions capture the nonlinearity in the unsteady pitching moment. Their magnitudes generally increase with increasing the Mach number, thereby implying that the flow is increasingly nonlinear as the Mach number increases.

Figures 23(a) and (b) show the plots of the amplitude correction function T_h and the phase correction function V_h for the non-circulatory pitching moment versus the Mach number, respectively. The amplitude correction is larger for the unsteady pitching moment than for the unsteady lift coefficient. The values of the phase correction V_h for both the pitching motion and plunging motion follow the same trend but with a small offset.

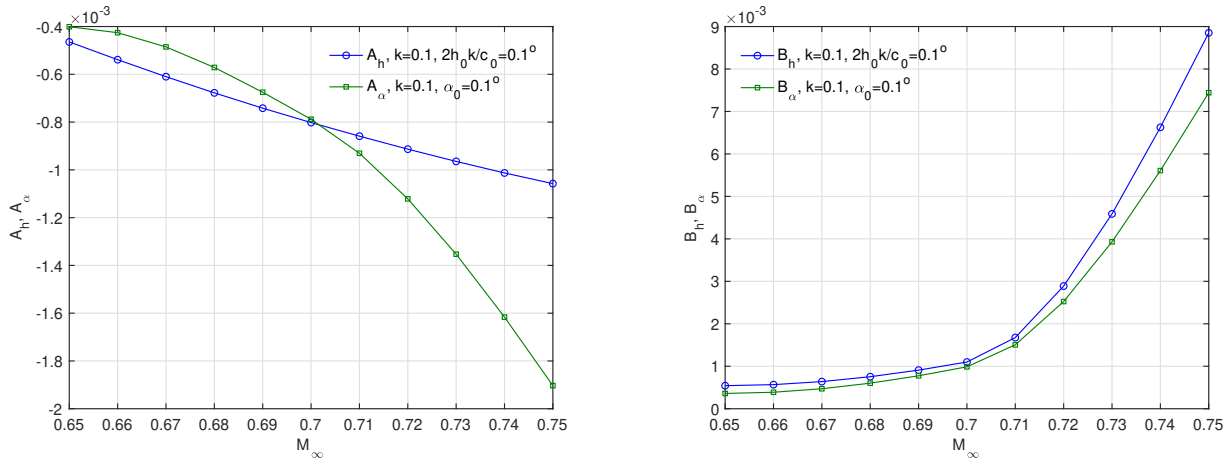

Figure 22. TTBW MAC Airfoil Transonic Correction Functions A_h and B_h for Aerodynamic Center Motion versus Mach Number for $k = 0.1$ and $\alpha_0 = \frac{2h_0 k}{c} = 0.1^\circ$

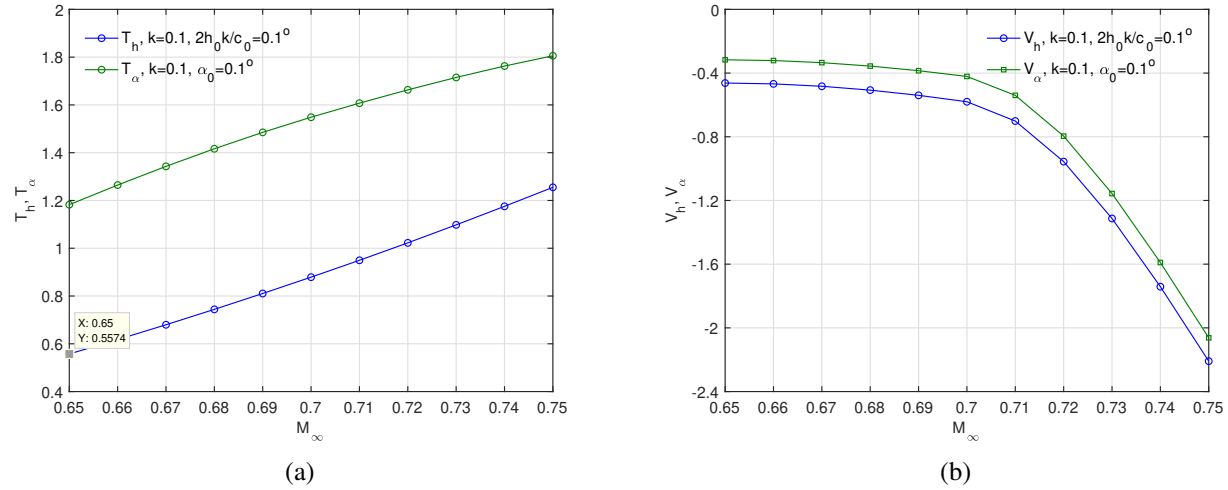

Figure 23. TTBW MAC Airfoil Transonic Correction Functions T_h and V_h for Aerodynamic Center Motion versus Mach Number for $k = 0.1$ and $\alpha_0 = \frac{2h_0 k}{c} = 0.1^\circ$

V. Transonic Airfoil Flutter Analysis

To illustrate the transonic correction method for use in flutter analysis, a simple illustrative flutter analysis is conducted. Consider a two-dimensional airfoil attached to a pair of elastic springs in translation and rotation as shown in Fig. 24.

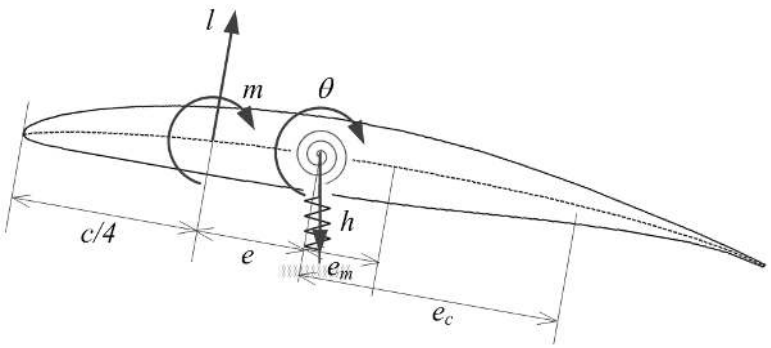

Figure 24. Airfoil in Pitch and Plunge

The equations of motion of the airfoil are described by

$$m\ddot{h} + me_{cg}\ddot{\alpha} + k_h(1+ig_h)h = -q_\infty c\tilde{c}_l \tag{64}$$

$$me_{cg}\ddot{h} + I\ddot{\alpha} + k_\alpha(1+ig_\alpha)\alpha = q_\infty c^2\tilde{c}_m \tag{65}$$

We assume $\bar{\alpha} = 0$ so that $\alpha = \tilde{\alpha}$. For simplification, we also assume zero structural damping so that $g_h = g_\alpha = 0$. The equations of motion are expressed in the frequency domain as

$$\begin{aligned}\mu\frac{d^2h}{d\tau^2} + \mu e_{cg}\frac{d^2\alpha}{d\tau^2} + \mu k_h^2 h =& -(U_h + iW_h)c_{l_\alpha}\left[C(k)\,2\frac{dh}{d\tau} + \frac{d^2h}{d\tau^2}\right] \\ & -(U_\alpha + iW_\alpha)c_{l_\alpha}c\left[C(k)\left(\alpha + 2\frac{e_c}{c}\frac{d\alpha}{d\tau}\right) + \frac{1}{2}\frac{d\alpha}{d\tau} + \frac{e_m}{c}\frac{d^2\alpha}{d\tau^2}\right]\end{aligned} \tag{66}$$

$$\begin{aligned}\mu e_{cg}\frac{d^2h}{d\tau^2} + \mu r^2\frac{d^2\alpha}{d\tau^2} + \mu r^2 k_\alpha^2\alpha =& c\left[\frac{\bar{e}}{c} - (A_h + iB_h)\frac{1}{h_0 k}\frac{dh}{d\tau}\right](U_h + iW_h)c_{l_\alpha}C(k)\,2\frac{dh}{d\tau} \\ & -c^2(T_h + iV_h)\,2\pi\frac{e_m}{c}\frac{1}{c}\frac{d^2h}{d\tau^2} \\ & +c^2\left[\frac{\bar{e}}{c} - (A_\alpha + iB_\alpha)\frac{\alpha}{\alpha_0}\right](U_\alpha + iW_\alpha)c_{l_\alpha}C(k)\left(\alpha + 2\frac{e_c}{c}\frac{d\alpha}{d\tau}\right) \\ & -c^2(T_\alpha + iV_\alpha)\left[\pi\frac{e_c}{c}\frac{d\alpha}{d\tau} + \frac{\pi}{16}\left(1 + 32\frac{e_m^2}{c^2}\right)\frac{d^2\alpha}{d\tau^2}\right]\end{aligned} \tag{67}$$

where $k_h = \frac{\omega_h c}{4V_\infty}$, $k_\alpha = \frac{\omega_\alpha c}{4V_\infty}$, $\mu = \frac{m}{m_a}$, $r_\alpha^2 = \sqrt{\frac{I}{m}}$, $m_a = \frac{\pi}{4}\rho_\infty c^2$.

To conduct the flutter analysis, the nonlinear terms are neglected. Let $x_1 = h$, $x_2 = \alpha$, $x_3 = \frac{dh}{d\tau}$, and $x_4 = \frac{d\alpha}{d\tau}$. We express the system of the second-order equations in a form of a system of first-order equations as

$$\mathbf{M}\frac{d\mathbf{x}}{d\tau} = \mathbf{S}\mathbf{x} \tag{68}$$

where

$$\mathbf{M} = \begin{bmatrix} 1 & 0 & 0 & 0 \\ 0 & 1 & 0 & 0 \\ 0 & 0 & \mu + (U_h + iW_h)c_{l_\alpha} & \mu e_{cg} + (U_\alpha + iW_\alpha)c_{l_\alpha}e_m \\ 0 & 0 & \mu e_{cg} + (T_h + iV_h)2\pi e_m & \mu r^2 + (T_\alpha + iV_\alpha)2\pi\left(\frac{c^2}{32} + e_m^2\right) \end{bmatrix} \tag{69}$$

$$\mathbf{S} = \begin{bmatrix} 0 & 0 & 1 & 0 \\ 0 & 0 & 0 & 1 \\ -\mu k_h^2 & -(U_\alpha + iW_\alpha)c_{l_\alpha}C(k)\,c & -2(U_h + iW_h)c_{l_\alpha}C(k) & -(U_\alpha + iW_\alpha)c_{l_\alpha}\left[2C(k)\,e_c + \frac{c}{2}\right] \\ 0 & -\mu r^2 k_\alpha^2 + (U_\alpha + iW_\alpha)c_{l_\alpha}C(k)\,c\bar{e} & 2(U_h + iW_h)c_{l_\alpha}C(k)\,\bar{e} & 2(U_\alpha + iW_\alpha)c_{l_\alpha}C(k)\,\bar{e}e_c - (T_\alpha + iV_\alpha)\pi c e_c \end{bmatrix} \tag{70}$$

We fix $k = 0.1$. Then, c_{l_α}, $\bar{e}$, and all the transonic correction functions are Mach number dependent. At each Mach number, the quantity μ is varied until the system is at neutral stability. For a given mass m, the dynamic pressure can be determined. For the illustrative problem, we choose $c = 9.1908$ ft, $\frac{e_{cg}}{c} = 0.15$, $\frac{e_m}{c} = 0.25$, $\frac{e_c}{c} = 0.5$, $r = 0.45c$, $k_h = 0.09$, $k_\alpha = 0.11$, and $m = 2.25$ slug/ft. Figure 25 shows the computed flutter boundary. The dynamic pressure at which flutter occurs decreases precipitously as the Mach number increases.

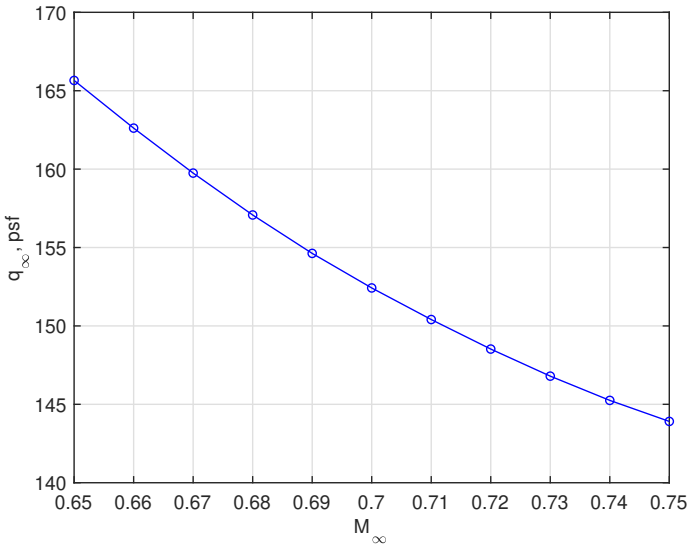

Figure 25. Flutter Boundary with Transonic Correction

This illustrative problem demonstrates a possible procedure for conducting flutter analysis for a full aircraft configuration. Unsteady RANS CFD simulations can be conducted for several airfoil sections at various wing stations. Transonic correction functions are then computed for these airfoil stations with the attendant sweep angle correction to the freestream Mach number. The generalized aerodynamic forces are next obtained by applying the generalized displacements computed by a finite-element structural dynamic model. This procedure could reduce the computational cost of conducting a three-dimensional unsteady RANS CFD simulations for a full configuration.

VI. Conclusions

This paper presents a transonic correction method for an oscillating airfoil in pitch and plunge. The proposed method applies correction functions to the Theodorsen's theory to capture the transonic nonlinear aerodynamics. These correction functions apply corrections to the amplitudes and the phase angles of the unsteady lift and pitching moment coefficients. Generally, the lift coefficient is quite linear, but the pitching moment coefficient exhibits high degree of nonlinearity even when the lift coefficient is linear. The proposed method postulates that this nonlinear behavior could be due to the moving shock which causes the aerodynamic center to also move. A correction is applied in the proposed method to capture the postulated motion of the aerodynamic center. A series of unsteady RANS CFD simulations of the airfoil at the mean aerodynamic chord of the Transonic Truss-Braced Wing aircraft are conducted using FUN3D. The data are used to compute these transonic correction functions as functions of the reduced frequency and Mach number. The computed responses of the unsteady lift and pitching moment coefficients using these transonic correction functions match the CFD simulation results very well even when the pitching moment coefficient is highly nonlinear. The effects of the amplitude of oscillation and mean angle of attack on the transonic correction are examined. When the airfoil is in the linear aerodynamic regime, the amplitude of oscillation and small change in the mean angle of attack do not seem to have a strong influence on the transonic correction functions. A flutter analysis of an airfoil in pitch and plunge illustrates the potential use of the proposed transonic correction method.

Acknowledgment

The authors wish to acknowledge NASA Advanced Air Transport Technology project for the funding support of this work. The authors also acknowledge Boeing Research and Technology and in particular Christopher Droney, Neal Harrison, Michael Beyar, Eric Dickey, and Anthony Sclafani, along with the NASA technical POC, Gregory Gatlin, for their research conducted under the NASA BAART contracts NNL10AA05B and NNL16AA04B. The research published in this paper is made possible by the technical data and wind tunnel test data furnished under these BAART contracts.

References

[1]Albano, E. and Rodden, W., "A Doublet-Lattice Method for Calculating Lift Distributions on Oscillating Surfaces in Subsonic Flows," AIAA Journal, Vol. 7, No. 2, February 1969, pp. 279-285.

[2]Bartels, R. E. and Stanford, B. K., "Aeroelastic Optimization with an Economical Transonic Flutter Constraint Using Navier-Stokes Aerodynamics," Journal of Aircraft, Vol. 55, No. 4, July 2018.

[3]Opgenoord, M., Drela, M., and Willcox, K., "Physics-Based Low-Order Model for Transonic Flutter Prediction," AIAA Journal, Vol. 56, No. 4, 2018.

[4]Theodorsen, T., "General Theory of Aerodynamic Instability and the mechanism of Flutter", NACA Report No. 496, 1949.

[5]Bradley, M. K. and Droney, C. K., "Subsonic Ultra Green Aircraft Research: Phase I Final Report," NASA Contractor Report NASA/CR-2011-216847, Boeing Research and Technology, April 2011.

[6]Bradley, M. K., Droney, C. K., and Allen, T. J., "Subsonic Ultra Green Aircraft Research Phase II: N+4 Advanced Concept Development," NASA Contractor Report NASA/CR-2012-217556, Boeing Research and Technology, May 2012.

[7]Nguyen, N., Fugate, J., Kaul, U., and Xiong, J., "Flutter Analysis of the Transonic Truss-Braced Wing Aircraft Using Transonic Correction," AIAA Structural Dynamics Conference, AIAA-2019-0217, January 2019.

[8]Kaul, U. and Nguyen, N., "RANS Simulations of a Pitching and Plunging VCCTEF Airfoil Toward a Transonic Flutter Model," AIAA Structural Dynamics Conference, AIAA-2019-2037, January 2019.

[9]Kaul, U. and Nguyen, N., "Extending A Correction Method for Unsteady Transonic Aerodynamics as Applied to Variable Camber Continuous Trailing Edge Flap," AIAA Applied Aerodynamic Conference, AIAA-2019-3157, June 2019.